Environmental Science: Atmospheres

ROYAL SOCIETY OF CHEMISTRY

PAPER

View Article Online
View Journal | View Issue

Cite this: *Environ. Sci.: Atmos.*, 2023, **3**, 35

Chemical characterization of prescribed burn emissions from a mixed forest in Northern Michigan†

Jamy Y. Lee,[a] Conner Daube,[b] Ed Fortner,[b] Nicholas Ellsworth,[a] Nathaniel W. May,[a] Jason Tallant,[c] Scott Herndon[b] and Kerri A. Pratt *[ad]

A prescribed burn was conducted in October 2017 at the University of Michigan Biological Station located in Pellston, Michigan. Approximately 0.025 km^2 of a temperate forest, primarily composed of red and white pine, red oak, bigtooth aspen, and red maple, were burned. The resulting smoke was sampled with a combination of real-time trace gas and aerosol instrumentation aboard the Aerodyne Mobile Laboratory. The resulting data were segmented into six plume periods, and the gas and particle concentration and composition measurements were characterized relative to modified combustion efficiency (MCE), which reflected both smoldering and flaming combustion. Emission factors for C_2H_2, C_2H_6, CH_4, and HCN were inversely related to MCE. The bulk submicron particle composition was characterized as mostly organic by mass (>92%). The majority of the bulk organic mass was within individual biomass burning particles (>93%, by number) in the accumulation mode. Analysis of the mass spectral ion peaks of individual biomass burning particles reveals two noteworthy signatures. First, red pine smoke contained combustion products of eugenol, released during the early stages of lignin combustion. Second, the combustion of northern hardwoods (*e.g.*, oak, aspen, maple) exhibited polycyclic aromatic hydrocarbons peaks corresponding to the combustion of furfural. The results from this study provide a detailed assessment of the composition of smoke emissions from biomass common to the understudied north-central United States.

Received 13th June 2022
Accepted 31st October 2022

DOI: 10.1039/d2ea00069e

rsc.li/esatmospheres

Environmental significance

Prescribed burns remove dry and dead vegetation that may contribute to high-severity wildfires and provide the opportunity for researchers to measure smoke emissions within a controlled environment. This study measured the gases and particles emitted from a prescribed burn in Michigan. In the north-central United States, prescribed burns occur more frequently than wildfires, but they are not commonly studied. The gases emitted followed trends previously observed in laboratory and field studies of pine wood. Key chemical differences were observed between the smoke particles emitted from softwood and hardwood combustion, highlighting the need for more studies in this region. These results can be incorporated into emission inventories used to inform future air quality and climate models and policies.

1. Introduction

Wildfires have become more frequent and severe in the past three decades.[1,2] Moreover, North American fire activity is projected to climb due to rising global temperatures and drought.[2–5] The multi-year trend in total area burned during wildfires has increased by 3.5% per year in California. Emissions from fires impact air quality,[5,7–9] health,[1,10] and climate.[11,12] Prescribed burns are used to minimize risks of high severity wildfires through staged controlled burns of excess dry fuel sources.[1,13,14] As of 2019, the number of acres burned from prescribed burns exceeded the total amount of acres burned due to wildfires in the United States.[16]

Prescribed burns provide a controlled environment to study atmospheric emissions from fires. The total area burned during prescribed fires in the central and southeastern United States is approximately equal to the total area burned during western United States wildfires.[1] Prescribed burns, however, typically emit lower concentrations of $PM_{2.5}$ (particulate matter below 2.5 μm in diameter) than wildfires.[1] $PM_{2.5}$ and gases emitted from fires vary widely by region, fuel type, density, and burning

[a]*Department of Chemistry, University of Michigan, Ann Arbor, MI, USA. E-mail: prattka@umich.edu*
[b]*Aerodyne Research Inc., Billerica, MA, USA*
[c]*Department of Ecology and Evolutionary Biology and Biological Station, University of Michigan, Ann Arbor, Pellston, MI, USA*
[d]*Department of Earth & Environmental Sciences, University of Michigan, Ann Arbor, MI, USA*

† Electronic supplementary information (ESI) available. See DOI: https://doi.org/10.1039/d2ea00069e

conditions.[19–22] Gas and particle emissions from prescribed burns in the western[20,23,24] and southeastern[15,17,20,25] regions of the United States have been characterized by comparing fuel types (*i.e.* chaparral, montane, pine trees) and burn conditions (smoldering or flaming combustion). Despite the vast number of studies on fire emissions, the mixed temperate forest located in the central United States is understudied.[1,21]

Emissions based on fuel type and burn conditions have been studied extensively in laboratory settings. Studies of over 300 vegetation species commonly found in the southeastern and southwestern United States have identified over 200 different gases emitted in fresh smoke.[17] To compare gas emissions from different vegetation and fires, emission factors (EFs) are calculated to estimate the mass of emitted species per mass of dry biomass consumed.[27] The modified combustion efficiency (MCE) quantifies differences in combustion efficiency based on emitted CO_2 and CO levels.[28] Generally, flaming combustion emits fully combusted species, such as CO_2, SO_2, and nitrogen containing species (NO, NO_2, and N_2O), whereas the relative amounts of CO, CH_4, and NH_3 are greater during smoldering combustion.[19,29] Furthermore, aerosols produced from fresh biomass burning vary in size and composition.[12] While carbonaceous aerosols dominate the $PM_{2.5}$ emissions from biomass burning, the type of combustion impacts aerosol chemical composition. Smoldering combustion generates organic carbon aerosol, while flaming combustion produces elemental carbon aerosol.[6]

Comprehensive EF and MCE values are essential for evaluating and predicting atmospheric impacts from fires.[29–31] These values depend on vegetation, location, and meteorological conditions underscoring the importance of extending laboratory measurements to a wide range of fire environments.[19–21,32] Field smoke measurements have been carried out through stationary[15,17] and mobile[33,34] ground-based methods, as well as airborne studies.[20,23,35,36] Stationary measurements have primarily occurred in the western and southeastern United States, integrating multiple types of vegetation representative of different forest ecosystems, with results that differed from laboratory measurements of similar vegetation.[20,23,35,36] Mobile platforms can measure pollutants directly downwind of fresh biomass burning plumes from prescribed burns,[34] and map the distribution of gas and particle emissions across local communities.[37] Results from stationary and mobile field campaigns have been compiled in emission inventories, aiding in the development of fire and smoke models.[38] Overall, field sampling of prescribed burns provide insights into how pre- and post-fire conditions, including fuel moisture, fire behavior, and meteorology, affect the resulting gas and particle emissions,[15] allowing connections to wildfires.

In this study, we used a combination of gas and particle instrumentation to characterize fresh biomass burning emissions from a prescribed burn near Pellston, Michigan. The burn occurred in a small section of a temperate forest (~41 km^2 total) composed of both deciduous and coniferous trees, representative of fuels common to the north-central United States.[39–41] Using real-time measurements on a mobile laboratory platform, we documented the varying atmospheric trace gas and aerosol concentrations as the prescribed burn progressed. Both bulk aerosol and single-particle measurements were conducted for a detailed chemical characterization of the aerosols emitted from the mixed forest.

2. Methods

2.1 Prescribed burn sampling

A prescribed burn and subsequent sampling were conducted on October 10, 2017 at the University of Michigan Biological Station (UMBS) (45°35′N 84°43′W) near Pellston, Michigan. Weather conditions were recorded at the Pellston Regional Airport of Emmett County Station (KPLN), approximately 7 km west of the prescribed burn area, and meteorological conditions were retrieved from Weather Underground (**https://www.wunderground.com/weather/us/mi/brutus/KPLN**, last accessed: 02/25/2022). During the measurement period (11:45–18:00 Eastern Daylight Time (EDT), local time), the meteorological conditions remained relatively constant with moderate temperatures (11–15 °C), moderate wind speeds (3–5 m s^{-1} from the north-northwest), relative humidity values of 44–61%, and fair skies. Gas and aerosol emissions were sampled with a suite of instrumentation installed within the Aerodyne Mobile Laboratory (AML) that drove <1 km downwind of the three burn plots, as shown in Fig. 1. The AML is a custom modified box truck designed to serve as a platform to enable real-time ambient air sampling while stationary or in motion.[42,43] On-board the mobile lab, instrument infrastructure, such as vacuum, networking, compressed zero air, and data storage, was powered *via* generators. Real-time data collection and visualization were used to direct the measurement activity. Instrument racks were shock mounted minimizing impacts from vibration and motion on instrument noise performance. Various inlets continuously sampled air at the front of the vehicle, separated from lofted exhaust pipes (generator and truck motor) at the rear. On-board GPS and anemometer units were used to calculate true wind speed while in motion. Data potentially

Fig. 1 Map depicting the locations of the three plots burned during the prescribed burn. Sampling occurred along Riggsville Road. Imagery and map data were adapted from Landsat/Copernicus and Google Earth, respectively. Copyright 2021.

Table 1 Plot number, fuel description, and estimated times of first and last ignition

Plot #	Fuel description	First ignition time (EDT)	Last ignition time (EDT)
1	Red pine with minor contributions of red oak, red maple, white pine, bigtooth aspen, and paper birch	13:25	15:30
2	Leafy debris and red pine needles with minor contributions of red oak leaves and bracken fern leaves	13:45	14:30
3	Northern hardwood forest primarily composed of red oak, big tooth aspen, white pine, and red maple as mixed slash	14:52	16:15

influenced by AML exhaust emissions were not included in any analysis presented herein.

The prescribed burn occurred on a long-term chronosequence research plot.[41,44] These research plots were within a regrown forest after a cut and burn treatment in 1911. Since 1911, these plots have been cut and burned at a successional timescale, providing researchers with long-term datasets linking the effects of climate, ecological, and biogeochemical controls to an upper Michigan forest. Approximately 0.025 km^2 of land containing both deciduous (red oak, red maple, bigtooth aspen, and paper birch) and coniferous trees (red and white pine) at the University of Michigan Biological Station were separated into three plot sections (Fig. 1, Table 1) and ignited by drip torches containing a mix of diesel and unleaded gasoline.

2.2 Gas analysers

Nitrous oxide (NO) was measured with 1 s resolution by a model 42i NO–NO_2–NO_x analyzer (Thermo Scientific, Waltham, MA, USA). Since interferences from additional nitrogen species can occur when using a molybdenum oxide catalyst,[45] the instrument was operated in "NO-mode". O_3 was measured with 2 s resolution by a model 202 ozone monitor (2B Technologies, Boulder, CO, USA). CO_2 was measured at 1 s resolution using a LI-6262 CO_2/H_2O analyzer (LI-COR Biosciences, Lincoln, NE, USA). Three compact tunable infrared laser differential absorption spectrometers (TILDAS, Aerodyne Research Inc., Billerica, MA, USA) collectively measured HCN, C_2H_2, CH_4, C_2H_6, N_2O, and CO with 1 s resolution.[46,47] Gas-phase instruments sampled from a forward-facing inlet (10 mm I.D. PFA) with a flow rate of ~8 L min^{-1}. All trace gas measurements were averaged to 20 s for analysis.

2.3 Real-time measurements of aerosols

Total particle number concentrations were measured with an ultrafine condensation particle counter (UCPC, model 3776, TSI, Inc., Shoreview, MN, USA). The UCPC measured particles ranging from 0.04 to 2.5 μm aerodynamic diameter with 1 s time resolution at a flow rate of 1.5 L min^{-1}. The particle number concentration and a Couette Centrifugal Particle Mass Analyzer were used to calibrate the mass concentration for refractory black carbon (rBC) measured with the Soot Particle Aerosol Mass Spectrometer (SP-AMS).

2.3.1 Soot particle aerosol mass spectrometer (SP-AMS). An Aerodyne SP-AMS measured the diameter (0.04–1 μm) and bulk chemical composition of submicron non-refractory particulate matter and refractory black carbon. Details of the SP-AMS are described elsewhere.[48–50] Briefly, aerosols are sampled with a volumetric flow rate of ~85 cm^3 min^{-1} and focused into a narrow beam by an aerodynamic particle focusing lens. Particle sizing was determined as particles passed a chopper when the AMS was in particle time-of-flight (PToF) mode. Non-refractory organics, nitrate, sulfate, ammonium, and chloride were vaporized by surface impaction on a heater at 600 °C. Refractory black carbon-containing particles were heated and vaporized by passing through a 1064 nm laser beam reaching temperatures surpassing 4000 K. Once vaporized, resulting gas phase molecules were ionized with 70 eV electron impact ionization. Ions formed were detected by a time-of-flight mass spectrometer. The AMS was typically run in Fast Mass Spec (FMS) mode, producing 1 s time-resolved mass concentrations (μg m^{-3}) for non-refractory organics, nitrate, sulfate, ammonium, chloride, and refractory black carbon. When the AML was stationary, the AMS was operated in FMS and PToF modes allowing for both the speciation and sizing of particles typically with 20 s time resolution. Emission ratios (ERs) for the SP-AMS measured aerosol components measured by the SP-AMS were calculated by dividing the average mass concentration for each aerosol component by the average mass concentration of CO.[51]

2.3.2 Aerosol time-of-flight mass spectrometer (ATOFMS). An ATOFMS measured the diameter and chemical composition of individual atmospheric particles in real-time.[52,53] Briefly, aerosols were introduced into an aerodynamic lens system at a flow rate of 0.1 L min^{-1}. The velocity of each single particle was measured by the time to traverse two continuous wave lasers, 405 and 488 nm (OBIS LX, Coherent Inc., Santa Clara, CA, USA), spaced 6 cm apart. Particle velocity was then used to calculate vacuum aerodynamic particle diameter based on a calibration curve of polystyrene latex spheres (Polysciences, Inc., Warrington, PA, USA) of known diameters (0.09–2 μm) and density (1 g cm^{-3}). Particles then entered a dual-polarity reflectron time-of-flight mass spectrometer (Tofwerk AG, Thun, Switzerland), where they were individually desorbed and ionized by a Q-switched 100 Hz 266 nm Nd:YAG laser (Centurion, Quantel USA Inc., Bozeman, MT, USA). The resulting positive and negative ion mass spectra correspond to a single laser-ablated particle. Mass spectra were analysed using FATES, a MATLAB-based toolkit.[54] Mass spectra were clustered based on similarity using an ART-2a neural network algorithm with a vigilance factor of 0.85, a learning rate of 0.05, and 20 iterations.[55] The resulting clusters were manually combined based on similarity to previously identified particle types,[56] including using ion markers associated with biomass burning particles.[57–59] In total, 20 117 individual particles were chemically analyzed by the ATOFMS during the ~7 h sampling period aboard the AML. 5894 particles (primarily ranging from 0.15–0.60 μm in

vacuum aerodynamic diameter) out of the 20 117 total particles measured occurred during the six smoke plume periods, defined in Section 2.5.

2.4 Calculations of modified combustion efficiency (MCE) and emission factors (EFs)

To evaluate burn conditions during sampling, the MCE was calculated, based on the equation defined by Ward and Radke,[28] for each plume sampling period using eqn (1):

$$\mathrm{MCE} = \frac{\Delta CO_2}{\Delta CO_2 + \Delta CO} \quad (1)$$

Here, ΔCO_2 and ΔCO are defined as the mole ratios of CO_2 and CO, respectively, measured during a smoke plume period minus the background mole ratio measured prior to the prescribed burn.

To quantify the variations in trace gas emissions, EFs were calculated in units of grams of compound per kilogram of dry biomass burned for CO, CO_2, C_2H_6, C_2H_2, CH_4, HCN, NO, and N_2O. EFs were calculated based on the carbon mass balance method,[27] assuming that the mass fraction of carbon in the dry biomass was 0.50,[27,29] and that the majority of volatized carbon was emitted as CO_2, CO, and CH_4, since other carbon-containing compounds contribute less than 5% of total carbon in EF calculations.[14,21,27] Brief (20 s average) time points with lower CO_2 or CO mole ratios compared to background levels were omitted from EF calculations, since they do not reflect smoke plume sampling.

2.5 Smoke plume identification

Prior to the ignition of the first plot (13:25 EDT), all instruments sampled ambient air while the AML was parked 2 km east of the burn site. The period from 11:45–12:44 EDT was identified as background, based on constant signals for the trace gas and particle measurements (except HCN and C_2H_2), and lack of contribution from local combustion emissions. HCN and C_2H_2 data were not available for this period due to an instrument error. Background concentrations for HCN and C_2H_2 were instead defined to be during 17:53–18:00 EDT, after plume sampling had concluded. Smoke plume periods, when the AML sampled smoke from the prescribed burn, were identified by an increase in total particle number concentrations, plus an increase in CO or CO_2 molar ratios, compared to the average background levels (11:45–12:44 EDT), for at least two consecutive minutes. Data that was potentially contaminated by vehicle and/or generator emissions, determined from observational notes and large concentration fluctuations, were excluded from the analysis.

3. Results and discussion

3.1 Prescribed burn conditions and trace gas emissions

Gas and particle measurements were made ~1 km south to southeast of the burn plots Fig. 1 when wind speeds were 3–5 m s^{-1}. Therefore, the smoke emissions for the measured plumes

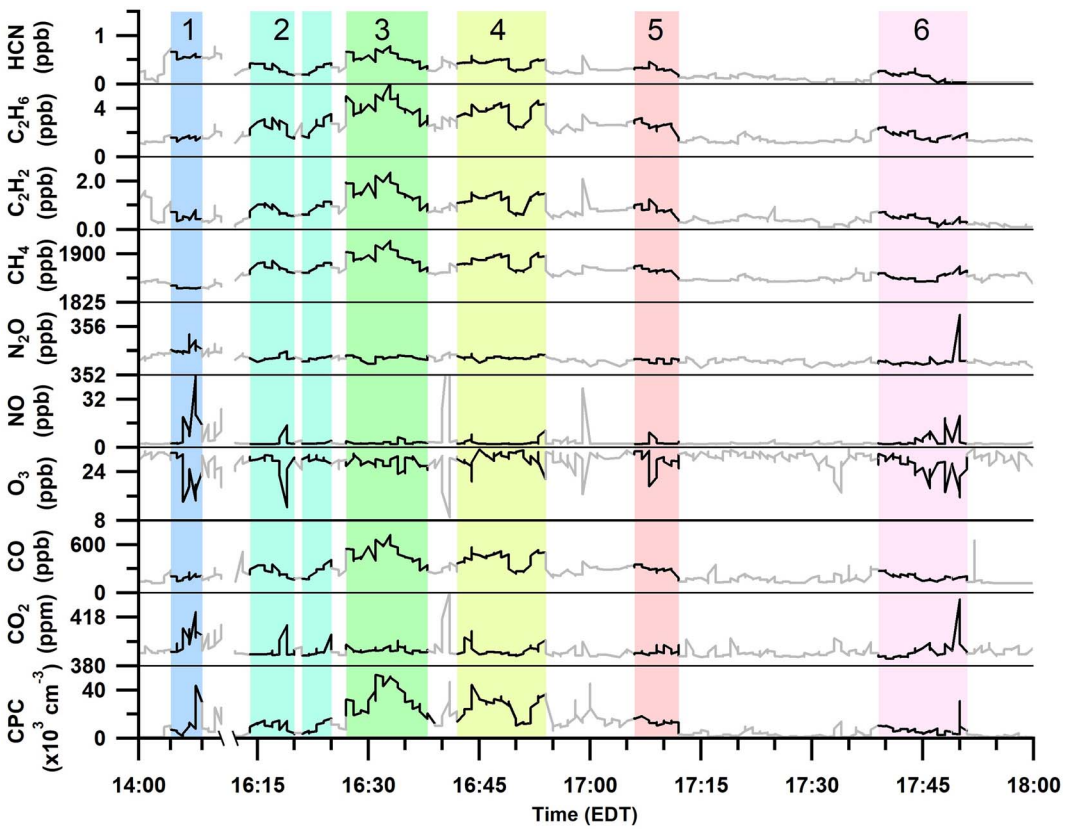

Fig. 2 Time series of 20 s averaged HCN, C_2H_6, C_2H_2, CH_4, N_2O, NO, O_3, CO, and CO_2 mole ratios and total particle (CPC) number concentrations over the full prescribed burn sampling period. Identified periods of smoke plume sampling are highlighted and numbered. Areas that are greyed out were not included in the plume analyses (Table 2).

Table 2 Plume times, corresponding plot number burned (Table 1), average MCEs, and compound-specific average EFs (g kg^{-1}) for the six plume periods with 95% confidence intervals reported

	Plume 1	Plume 2	Plume 3	Plume 4	Plume 5	Plume 6
Start time (EDT)	14:05:40	16:14:00	16:27:20	16:42:40	17:06:00	17:39:20
End time (EDT)	14:09:40	16:25:00	16:38:20	16:53:40	17:12:20	17:51:00
Plot #	1 & 2	3	3	3	3	3
MCE	0.993 ± 0.002	0.98 ± 0.02	0.87 ± 0.04	0.92 ± 0.04	0.95 ± 0.05	0.98 ± 0.01
Carbon dioxide (CO_2)	1821 ± 5	1780 ± 50	1570 ± 80	1670 ± 80	1740 ± 100	1790 ± 30
Carbon monoxide (CO)	8 ± 3	30 ± 30	150 ± 50	90 ± 50	60 ± 50	20 ± 20
Methane (CH_4)	N/A	4 ± 5	17 ± 5	10 ± 5	6 ± 6	4 ± 5
Ethane (C_2H_6)	0.03 ± 0.03	0.2 ± 0.2	0.8 ± 0.3	0.4 ± 0.2	0.3 ± 0.3	0.07 ± 0.04
Acetylene (C_2H_2)	0.06 ± 0.04	0.1 ± 0.2	0.6 ± 0.2	0.3 ± 0.2	0.2 ± 0.2	0.13 ± 0.08
Hydrogen cyanide (HCN)	0.09 ± 0.06	0.05 ± 0.06	0.21 ± 0.07	0.12 ± 0.06	0.09 ± 0.08	0.05 ± 0.04
Nitric oxide (NO)	1.6 ± 0.4	0.8 ± 0.3	1.7 ± 0.7	1.1 ± 0.4	1.2 ± 0.7	4 ± 2
Nitrous oxide (N_2O)	0.2 ± 0.1	0.07 ± 0.02	0.19 ± 0.07	0.14 ± 0.07	0.03 ± 0.02	0.3 ± 0.2

were ~3–5 min in age. The total particle number concentrations and trace gas mole ratios measured during the six smoke plume sampling periods are shown in Fig. 2 and Table 2.

Sampling of plume 1 occurred approximately 40 min after the first ignition of plot 1 and 20 min after the first ignition of plot 2 (Tables 1 and 2). The first burned plot (plot 1, Fig. 1) was primarily composed of red pine, with minor contributions from other mixed fuels (red oak, red maple, white pine, bigtooth aspen, and paper birch), and was ignited in the southeastern corner at 13:25 EDT; ignition of fuels continued intermittently until 15:30 EDT. The burning of the second plot overlapped in time with the burning of the first plot and consisted of similar vegetation as the first section except that the vegetation in the second plot was broken down as leafy debris and pine needles. Plot 2 failed to stay aflame beyond the initial ignition from the drip torches at 13:45 EDT and attempts to re-ignite the second plot stopped by 14:30 EDT. In general, plots 1 and 2 burned with low to moderate severity, consuming less than 40% of the available fuel.

Plumes 2–6 primarily overlapped with the burning of plot 3 and with contributions from the smoldering of plots 1 and 2. Plot 3 was ignited at 14:52 EDT and burned with higher severity than plots 1 and 2, consuming approximately 60% of the available fuels. This third and final burned plot contained a diverse hardwood slash mixture composed of red maple, red oak, and bigtooth aspen, as well as softwood white pine (Table 1, Fig. 1). Plume 2 began at the time of the final ignition of plot 3 (16:15 EDT), and subsequently, was likely most influenced by the ignition of the mixed slash from plot 3. Plumes 3 to 6 corresponded to emissions after all plots had been ignited and followed the spread of the burn as it rekindled and/or self-extinguished. Plot 3 continued to burn throughout the night, after air sampling had concluded.

The range of MCEs measured during the smoke sampling periods was 0.87–0.993 (Table 2). MCE values ranging from ~0.65–0.85 correspond to smoldering combustion, and a MCE near 0.99 describes a fire with primarily flaming combustion.[30] A fire with roughly equal contributions from smoldering and flaming combustion has a MCE near 0.9.[30] All six plume periods had average MCEs greater than 0.85, implying that all plumes had some or majority influence from flaming combustion. Plume 1 had the highest MCE (0.993 ± 0.002, Table 2), corresponding to primarily flaming emissions from the first and second plots. Plume 2 corresponded with the last ignition of plot 3, and this is reflected by a high MCE of 0.98 ± 0.02. Plumes 3 and 4 occurred after the last ignition as the fire intensity decreased, resulting in lower MCE values (0.87 ± 0.04 and 0.92 ± 0.04, respectively). Plumes 5 and 6 coincided with flare-ups, observed as the fire spread throughout plot 3 and as reflected by the increase in MCE values (0.95 ± 0.05 and 0.98 ± 0.01, respectively).

MCE values were inversely related with the average EFs for C_2H_6, C_2H_2, CH_4, and HCN shown in Fig. 3, as well as the total particle number concentrations (Table S1†). Average trace gas mole ratios and particle number concentrations for the six smoke plumes are provided in Table S1†. As described by Ward and Radke,[28] smoldering combustion produces higher total particle emissions, while flaming combustion produces fewer

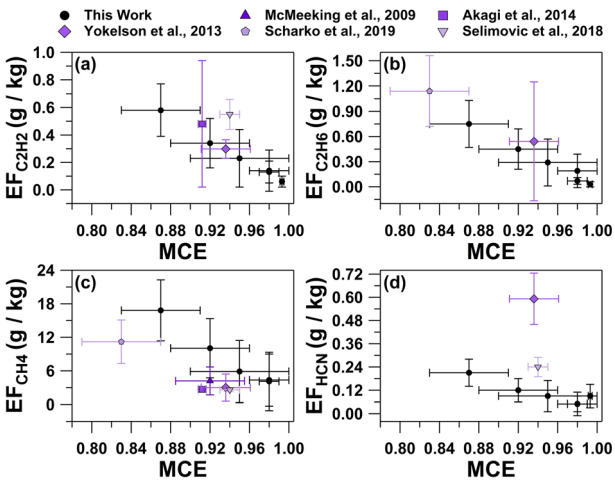

Fig. 3 Average emission factors for (a) C_2H_2, (b) C_2H_6, (c) CH_4, and (d) HCN *versus* MCE values for the six smoke plume periods, as well as previous studies. Error bars represent the 95% confidence interval for each calculated value. Previous values are from McMeeking *et al.*,[6] Akagi *et al.*,[15] Yokelson *et al.*,[17] Scharko *et al.*,[18] and Selimovic *et al.*[26]

total particles. This trend can often be observed in plume particle concentrations when sampling in close proximity to the fire source. Plumes 3, 4, and 5 had the lowest MCE values of all plume periods (0.87 ± 0.04, 0.92 ± 0.04, and 0.95 ± 0.05, respectively) and were characterized by having the largest total particle number concentrations (33 000 ± 4000 particles per cm^3, 26 000 ± 3000 particles per cm^3, and 14 000 ± 1000 particles per cm^3, respectively). Conversely, plumes 1, 2, and 6 had almost pure flaming MCE values (0.993 ± 0.002, 0.98 ± 0.02, and 0.98 ± 0.01, respectively) and lower total particle number concentrations (11 000 ± 7000 particles per cm^3, 10 000 ± 1000 particles per cm^3, and 7000 ± 2000 particles per cm^3, respectively). Not surprisingly, these total particle number concentrations that were significantly higher than background concentrations measured prior to the prescribed burn (1500 ± 900 particles per cm^3), which were similar to previous summertime measurements at this site (2000 ± 1000 particles per cm^3).[60] The particle concentrations during the lower MCE plume periods were on par with typical near-source particle concentrations for smoke plumes (>20 000 particles per cm^3).[61]

The range of ethane (C_2H_6) EFs (0.03–0.75 g kg^{-1}, Table 2) were similar to the average C_2H_6 EF calculated based on a mixture of lab and field measurements of a pine understory (0.5 ± 0.7 g kg^{-1}) collected from the southeastern and the southwestern United States.[17] Similarly, the acetylene (C_2H_2) EFs ranged from 0.06–0.58 g kg^{-1} (Table 2), which is consistent with previous prescribed burn measurements from pine forests in the southeastern United States (0.3 ± 0.1 g kg^{-1}, Akagi *et al.*[30] and 0.5 ± 0.5 g kg^{-1}, Akagi *et al.*[15]). However, the C_2H_2 EF can vary widely, as previously observed from a pine forest prescribed burn in the southeastern United States (7 ± 3 g kg^{-1})[18] and laboratory measurements of lodgepole pine collected from the western United States (1.9 ± 0.4 g kg^{-1})[26] that were significantly greater than the range measured in this study. The lower C_2H_2 EFs in this study compared to what was observed by Scharko *et al.*[18] and Selimovic *et al.*[26] may be associated with a difference in the pyrolysis temperature of the burn, as C_2H_2 EFs increase with higher burn temperature, as discussed by Scharko *et al.*[18] and references therein.

The methane (CH_4) EFs for plumes 2–6, which sampled smoke emissions after the ignition from all three plots, ranged from 4–17 g kg^{-1}. The CH_4 EFs were greater than previous laboratory and field measurements of pine tree fires with MCEs greater than 0.9 (CH_4 EFs of 2.68 ± 0.05 g kg^{-1}, Akagi *et al.*;[15] 4 ± 3 g kg^{-1}, McMeeking *et al.*;[6] 2.6 ± 0.3 g kg^{-1}, Selimovic *et al.*[26]). Methane molar ratios during plume 1, which correspond to the smoke released from plots 1 and 2, were not greater than background values. Plume 1 had the greatest MCE with near pure flaming contributions (0.993 ± 0.002), which may have contributed to the limited CH_4 emissions.[62]

The EFs for HCN (0.05–0.21 g kg^{-1}, Table 2) were significantly lower than previously reported (0.6–0.7 g kg^{-1}),[17,30,63] potentially related to HCN being primarily emitted during smoldering combustion.[15,64] For NO and N_2O, average EFs previously reported for temperate forests (3 ± 1 g kg^{-1} and 0.2 ± 0.2 g kg^{-1}, respectively)[30] fall within range of this study for NO and N_2O (0.8–4 g kg^{-1} and 0.03–0.2 g kg^{-1}, respectively, Table 2). Variability in these measurements is expected because the nitrogen content of the biomass fuel can influence the emissions of nitrogen-containing compounds.[23,65] Compared to the commonly studied vegetation (ponderosa pine, lodgepole pine, grass, peat, *etc.*) in previous studies from the southeastern and southwestern United States, the primary fuel burned here, red pine, has a lower nitrogen content.[66]

3.2 Characterization of particle composition from resulting smoke plumes

3.2.1 Bulk aerosol chemical composition. Submicron non-refractory aerosol composition and refractory black carbon mass concentrations measured by the SP-AMS were compared between the six plume periods in Fig. 4a. The average particle size distribution (Fig. S1†) was consistent with previous laboratory,[67] prescribed burn,[57] and wildfire[68,69] measurements of mixed vegetation combustion. The primarily red pine and northern hardwood forest vegetation in this prescribed burn produced large amounts of organic aerosol (>92%, by mass), consistent with previous laboratory measurements of ponderosa pine and lodgepole pine producing almost exclusively (>95%) organic aerosol, by mass.[20] For all plume periods, rBC contributed 3–5%, by mass (Fig. 4a), with OA/rBC ratios of 25–37 (Table S2†). The OA/rBC ratios were higher than previous laboratory studies of lodgepole pine (15–28).[67] Black carbon production is associated with flaming combustion.[6] Since all plume periods were classified as having some or all flaming contributions (MCEs between 0.87 – 0.993), the higher OA/rBC ratio is most likely due to the severity of the burn. Ammonium, sulfate, nitrate, and chloride each contributed less than or equal to 1% of the measured aerosol mass, with the exception of plume 6, when sulfate contributed 2% of the measured mass (Fig. 4a).

Chemically-resolved submicron aerosol ERs for the six smoke plumes are listed in Table S2†. Laboratory-produced PM_1 ERs are generally 0.5–14 times greater than PM_1 ERs from prescribed burns.[20,33,35,70] Similarly, the ERs for non-refractory OA and rBC were 10 and 3 times lower, respectively, than OA and rBC ERs from laboratory measurements of similar vegetation.[20] However, the range of OA ERs for this study (50–120 mg g^{-1}) was in line with previous mixed conifer forest prescribed burn studies from California (95–104 mg g^{-1}).[20] The range of rBC ERs for this study (2.2–4.5 mg g^{-1}) was lower than observed in the previous mixed conifer forest prescribed burn (5.5–5.8 mg g^{-1}),[20] most likely due to this low severity burn producing lower mass concentrations of rBC. Differences in PM_1, OA, and rBC ERs between laboratory and field measurements were attributed to fuel type, fuel moisture, and location.[20,33] ERs for sulfate, nitrate, ammonium, and chloride for the six plume periods were all below 1.3 mg g^{-1} (Table S2†).

Both O : C and H : C ratios for all plume periods were similar (ranges of 0.25–0.41 and 1.74–1.87, respectively, Fig. 4b) with no significant MCE dependence, in contrast to the linear MCE relationships observed by Heringa *et al.*[71] Fresh biomass burning emissions for various fuel types (*e.g.*, pine, spruce, *etc.*) have been previously observed to have similar O : C (0.18–0.48) and H : C ratios (1.34–1.7).[32,67,71] Plumes 1 and 6 had larger variations in O :

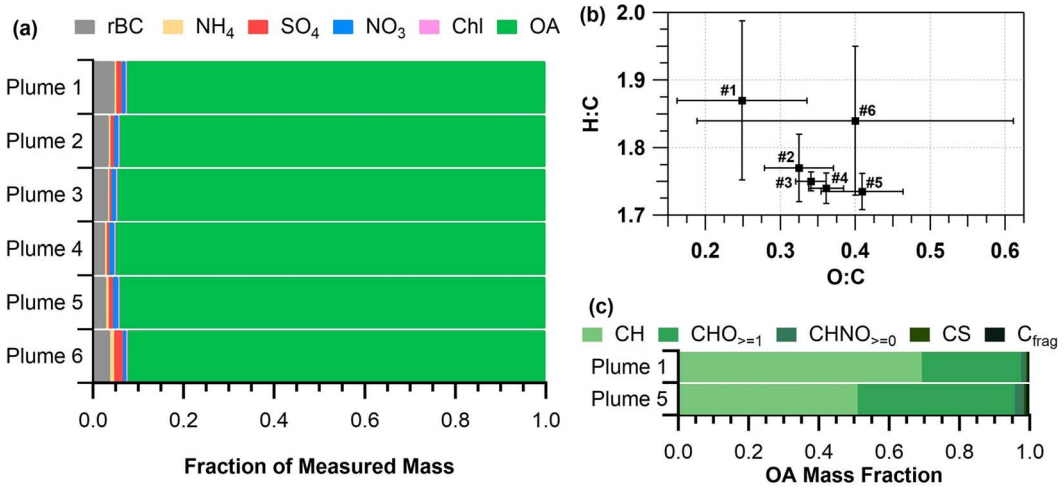

Fig. 4 (a) Mass fractions of submicron refractory black carbon (rBC), as well as non-refractory organic aerosol (OA), ammonium (NH_4), sulfate (SO_4), nitrate (NO_3), and chloride (Chl) for the six smoke plume periods during the prescribed burn, (b) Van Krevelen diagram depicting the average H : C and O : C ratios for each smoke plume, (c) fractional contributions to OA from hydrocarbon (CH), oxygenated ($CHO_{\geq 1}$), nitrogen-containing ($CHNO_{\geq 0}$), sulfur-containing (CS), and carbon fragments (C_{frag}).

C and H : C ratios (0.25 ± 0.09 and 1.8 ± 0.1 for plume 1 and 0.4 ± 0.2 and 1.8 ± 0.1 for plume 6, respectively) compared to plumes 2–5 (Fig. 4b). This is likely an indication of more intense burning during these two plumes compared to plumes 2–5. Sampling for plume 1 occurred while plots 1 and 2 were continually being ignited, resulting in an increase in non-oxygenated (higher H : C, lower O : C) organics from higher intensity burning. The average O : C ratio gradually increased through plumes 2–5 as the plots burned (Fig. 4b). In contrast, plume 6 sampled smoke while plot 3 flared-up part way through the measurement period, resulting in a large range of H : C and O : C ratios.

Plume 1 had a lower O : C ratio compared to plumes 2–6, as reflected in the higher OA mass fraction contribution of hydrocarbon (CH) ion signal shown in Fig. 4c. Fig. 4c shows the OA signal percentage by ion type (CH, $CHO_{\geq 1}$, $CHNO_{\geq 0}$, CS, and carbon fragments (C_{frag}) measured by the SP-AMS) normalized to the OA mass fraction (Fig. 4a), for plumes 1 and 5. Plumes 2–6, which all included the emissions from plot 3, were similar in OA composition to plume 5 (Fig. 4c and S2†), and thus plume 5 is discussed here as representative of plumes 2–6. Plume 5 had a higher contribution from oxygenated ($CHO_{\geq 1}$) and nitrogen-containing ($CHNO_{\geq 0}$) organics compared to plume 1 (Fig. 4c). The OA for plume 1 was composed of 69% hydrocarbon ion signal, 28% oxygenated species, and 1.5% nitrogen-containing organic species, by mass, whereas plume 5 was composed of 51% hydrocarbon ion signals, 45% oxygenated species, and 2.7% nitrogen-containing organic species, by mass. Sulfur-containing (CS) and carbon mass fragments (C_{frag}) made up fewer than 1% of the organic species, by mass, for both plumes. The average organic mass spectra for plumes 1–3, 5, and 6 are shown in Fig. S3.† A difference plot of the average OA mass spectra from plumes 1 and 5 is shown in Fig. S4,† illustrating an increased presence of oxygenated and nitrogen-containing compounds in plume 5. The oxygenated and nitrogen-containing organic species in plume 5 could be related to phenolic and nitrophenolic species.[72] This difference in chemical composition may be related to vegetation, as hardwoods (red oak, big tooth aspen, and red maple burned and sampled in plume 5) generally have higher nitrogen content,[73] and produce more phenolic compounds when combusted[74] than softwoods. Note that red pine was burned and sampled in plume 1. Previous studies have suggested that phenolic compounds contribute to secondary organic aerosol production as smoke plumes age.[75,76] Notably, nitrophenolic compounds from fires make up a significant portion of brown carbon.[72]

3.2.2 Individual particle chemical composition. Of the 5894 individual 0.13–2.5 μm aerosol particles chemically analyzed by the ATOFMS during the six smoke plume periods, $93.0 \pm 0.7\%$, by number, were classified as biomass burning. Since the SP-AMS measured >92% of the submicron aerosol mass as OA, the majority of the individual biomass burning particles measured by the ATOFMS consisted of OA, by mass. The majority of the remaining ATOFMS individual particles were classified as organic carbon-nitrate-sulfate (Fig. S5†), as described in the ESI.†

The average ATOFMS single-particle mass spectrum for all measured biomass burning particles during the prescribed burn is shown in Fig. 5. This is consistent with previously observed biomass burning particles measured by ATOFMS.[57–59,77] The mass spectra are characterized by dominant potassium (m/z 39 (K^+)), sulfate (m/z −97 (HSO_4^-)), and nitrate (m/z −46 (NO_2^-) and −62 (NO_3^-)) peaks.[57,59] Potassium accounts for less than 5% of smoke particle mass,[61] but is a common tracer of biomass burning particles[6,77,78] that is easily ionized by laser desorption/ionization.[79] These freshly emitted biomass burning particles also included elemental carbon (m/z 12 (C^+), 24 (C_2^+), C_n^+, …; −24 (C_2^-), −36 (C_3^-), C_n^-, …), consistent with soot from flaming combustion.[80] In addition, organic aerosol markers[59,81,82] characteristic of smoldering combustion were present, including organic carbon (m/z 27 ($C_2H_3^+$), 37 (C_3H^+), and 43 ($C_2H_3O^+/C_3H_7^+$)) and organic nitrogen (m/z 27 (NCH^+), 43 ($CHNO^+$), −26 (CN^-), and −42

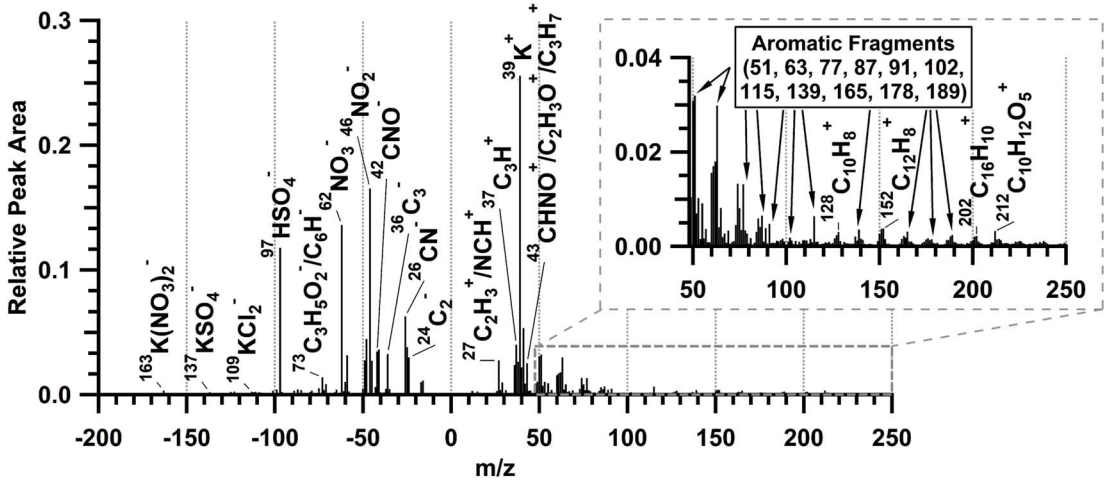

Fig. 5 ATOFMS average positive and negative ion mass spectrum of 5500 freshly emitted biomass burning particles sampled during plumes 1–6.

(CNO^-)) markers. The average negative ion mass spectrum contains fresh biomass burning markers including levoglucosan fragments (m/z −73 ($C_3H_5O_2^-$), −71 ($C_3H_3O_2^-$), −59 ($C_2H_3O_2^-$), −45 (CHO_2^-)),[58,59] and potassium salt clusters (m/z −163 ($K(NO_3)_2^-$), −137 (KSO_4^-), and −109 (KCl_2)).[57] Fewer than half of the individual biomass burning particles, by number, (Fig. S6†) contained polycyclic aromatic hydrocarbons (PAHs)[83,84] and aromatics measured as ion peaks at m/z 51, 63, 77, 87, 91, 102, 115, 128, 139, 152, 165, 178, 189, and 202.[80,85–87]

The average ATOFMS individual biomass burning particle mass spectra for each plume period are shown in Fig. S7,† with similar mass spectra for plumes 2–6, and differing composition for plume 1, similar to that observed for the SP-AMS organic aerosol mass spectra. Therefore, the average biomass burning

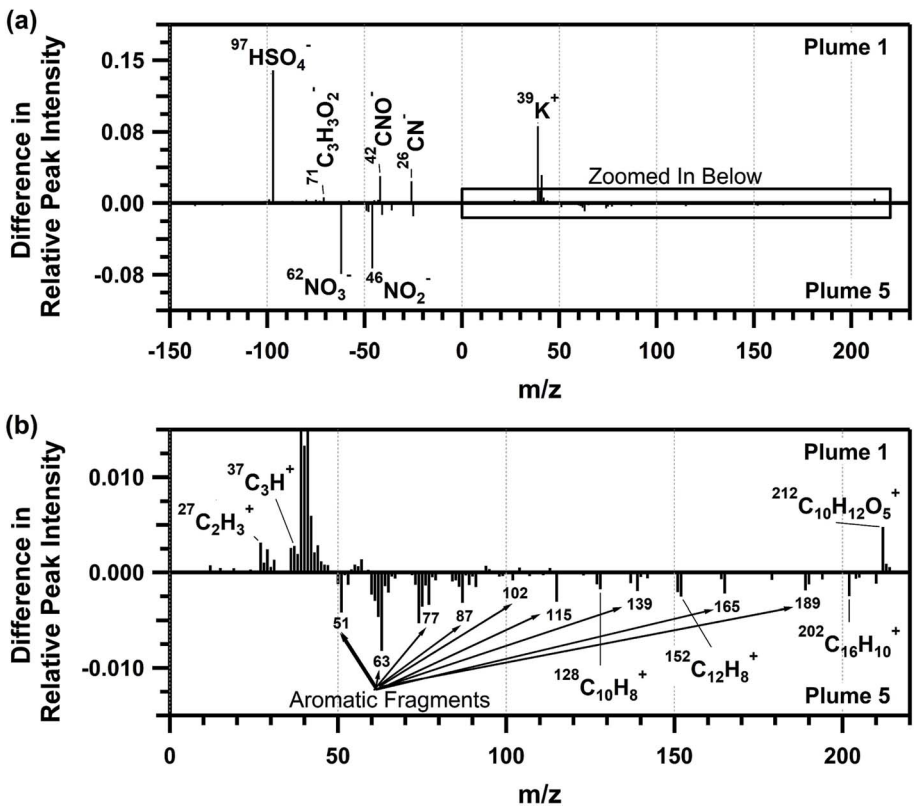

Fig. 6 (a) ATOFMS positive and negative ion mass average spectrum and (b) expanded positive ion mass spectrum for biomass burning particles during plume 5 subtracted from biomass burning particles during plume 1. Positive relative peak intensities correspond to greater abundance during plume 1; negative relative peak intensities correspond to greater abundance during plume 5. Only ion peaks above 95% confidence limits following subtraction are shown.

single-particle mass spectrum from plume 5 was compared to the average biomass burning particle mass spectrum from plume 1 and shown in Fig. 6. Plume 1 corresponded with the burn of plots 1 and 2, which contained primarily red pine, a softwood, whereas plume 5 corresponded with the burn of plot 3, containing a mixture of northern hardwood forest (*i.e.*, red oak, bigtooth aspen, and red maple, Table 1) with minor contributions from softwood species (*i.e.*, white pine, Table 1). Molecular ion peaks corresponding to the PAHs[80,85–89] naphthalene (m/z 128 ($C_{10}H_8^+$)), acenaphtylene (m/z 152 ($C_{12}H_8^+$)), and pyrene/fluoranthene (m/z 202 ($C_{16}H_{10}^+$)), as well as aromatic ion fragments (m/z 51, 63, 77, 87, 102, 115, 139, 165, 189), were more prominent in plume 5, compared to plume 1. The abundance of aromatic ion fragments observed by ATOFMS is consistent with the phenolic and nitrophenolic species observed in the SP-AMS spectrum for plume 5. As observed in previous single-particle mass spectrometry studies, naphthalene, acenaphtylene, and pyrene/fluoranthene are common PAHs released from the combustion of furfural, a common component of hardwoods.[88] High-density hardwoods are expected to burn longer and slower, leaving behind more unreacted wood mass compared to pine, a low-density softwood, when burned at the same pyrolysis temperature.[22,90,91] This is consistent with the increased presence of PAHs in the individual biomass burning particles measured during plume 5 (Table 1). In addition, the higher peak intensities for nitrate (m/z −46 (NO_2^-) and −62 (NO_3^-)) in the plume 5 biomass burning particles compared to plume 1 is consistent with the nitrate mass fractions measured by the SP-AMS (0.8 and 1.1% for plumes 1 and 5, respectively, Fig. 4a).

As shown in Fig. 6, the plume 1 biomass burning particles showed higher signals for potassium (m/z 39 (K^+)), organic carbon (m/z 27 ($C_2H_3^+$), 29 ($C_2H_5^+$), and 37 (C_3H^+)), sulfate (m/z −97 (HSO_4^-)), organic nitrogen (m/z −26 (CN^-), −42 (CNO^-)), levoglucosan (m/z −73 ($C_3H_5O_2^-$), −71 ($C_3H_3O_2^-$), −59 ($C_2H_3O_2^-$), −45 (CHO_2^-)), and an aromatic peak at m/z 212 ($C_{10}H_{12}O_5^+$)[89] that results from the combustion of eugenol.[83,88] The higher signals for the organic carbon fragments within plume 1, compared to plume 5, also agrees with the greater CH mass fraction observed by the SP-AMS (Fig. 4c). The larger sulfate signal for plume 1 compared to plume 5 aligns with the sulfate mass fractions measured by the SP-AMS (1.3 and 1.0% for plumes 1 and 5, respectively, Fig. 4a). With respect to m/z 212, eugenol is released during the early stages of lignin combustion and has a resulting mass spectrum similar to pine wood soot.[83,88] The higher contribution of this ion in plume 1 compared to plume 5 reflects the increased contribution of pine wood combustion during plume 1 (Table 1) and further highlights the influence fuel type has on the chemical composition of the emitted biomass burning particles.

4. Conclusions

Trace gas and aerosol particle emissions from a prescribed burn in Pellston, Michigan were measured within ~3–5 min following emission. Three plots, two containing primarily red pine and the third containing a mixture of northern hardwood (red oak, bigtooth aspen, and red maple) and white pine were burned sequentially. The measured emission factors for CH_4, C_2H_6, C_2H_2, and HCN were inversely related to MCE, as previously determined in laboratory pine studies. Lower CH_4 and C_2H_2 emission factors, compared to previous field measurements, may be explained by the low pyrolysis temperature of this burn.[18] CO_2, CO, C_2H_6, HCN, NO, and N_2O EFs did not significantly vary between plots, suggesting minimal fuel type influence, and followed trends explained by MCE.

The majority (93.0 ± 0.7%, by number) of the individual particles analysed by ATOFMS corresponded to biomass burning and were determined by SP-AMS to be mainly OA by mass. Throughout the prescribed burn, over 92% of the submicron aerosol mass was OA, consistent with laboratory and field measurements of pine wood combustion. OA/rBC ratios (25–37) were consistent with a lower severity burn that produced less rBC, by mass, compared to previous laboratory studies.[67] Biomass burning particles measured from the combustion of primary red pine displayed markers corresponding to eugenol soot. Particles measured from the combustion of the northern hardwoods (red oak, bigtooth aspen, and red maple) and white pine displayed PAH markers consistent with the combustion of furfural, and showed greater mass fractions of oxygenated and nitrogen-containing organic compounds. The prominence of PAH markers in the latter plume periods may be associated with the incomplete combustion of higher-density woods.[22,90,91] Previous field measurements in the western and southeastern United States had higher emission ratios of particulate OA and rBC than what was emitted in this Northern Michigan prescribed burn. However, the first two plots burned in this study occurred at low to moderate severity, which may have contributed to the lower rBC emission ratios. Additional biomass burning trace gas and aerosol particle studies are required to better understand the impacts of fires across different seasons, severity, and in this area of the United States.

Data availability

Data measured by the SP-AMS, TILDAS, TSI, 2B Tech, LI-COR, and Thermo Scientific instruments are archived through the CSL FIREX-AQ archive (**https://csl.noaa.gov/groups/csl7/measurements/2019firex-aq/AML/**). ATOFMS data are archived through the University of Michigan Library's Deep Blue Repository (**https://doi.org/10.7302/1dbr-2f25**).

Author contributions

CD, EF, NE, and NM conducted the measurements. JL, CD, EF, and JT conducted the formal analysis. KP and SH conceptualized and supervised the project. JL wrote the manuscript with contributions from KP, CD, and EF.

Conflicts of interest

There are no conflicts to declare.

Acknowledgements

The authors acknowledge the University of Michigan Biological Station and PlantWise, LLC for leading the prescribed burn and for research logistical support. Photos used to create the Table of Contents Entry are credited to Roger Hart and Michigan Photography. The authors acknowledge the University of Michigan Department of Chemistry for funding and the Pratt Lab and Aerodyne Research Inc. for their support. The Aerodyne Mobile Laboratory was supported by National Oceanic and Atmospheric Administration (Grant number: NA16OAR4310104). We thank Rachel Hems for helpful discussions.

References

1 D. A. Jaffe, S. M. O'Neill, N. K. Larkin, A. L. Holder, D. L. Peterson, J. E. Halofsky and A. G. Rappold, Wildfire and prescribed burning impacts on air quality in the United States, *J. Air Waste Manage. Assoc.*, 2020, **70**, 583–615.

2 P. E. Dennison, S. C. Brewer, J. D. Arnold and M. A. Moritz, Large wildfire trends in the western United States, 1984–2011, *Geophys. Res. Lett.*, 2014, **41**, 2928–2933.

3 M. Flannigan, A. S. Cantin, W. J. de Groot, M. Wotton, A. Newbery and L. M. Gowman, Global wildland fire season severity in the 21st century, *For. Ecol. Manage.*, 2013, **294**, 54–61.

4 A. L. Westerling, Increasing western US forest wildfire activity: sensitivity to changes in the timing of spring, *Philos. Trans. R. Soc., B*, 2016, **371**, 20150178.

5 A. P. Williams, J. T. Abatzoglou, A. Gershunov, J. Guzman-Morales, D. A. Bishop, J. K. Balch and D. P. Lettenmaier, Observed Impacts of Anthropogenic Climate Change on Wildfire in California, *Earth's Future*, 2019, **7**, 892–910.

6 G. R. McMeeking, S. M. Kreidenweis, S. Baker, C. M. Carrico, J. C. Chow, J. L. Collett Jr, W. M. Hao, A. S. Holden, T. W. Kirchstetter, W. C. Malm, H. Moosmüller, A. P. Sullivan and C. E. Wold, Emissions of trace gases and aerosols during the open combustion of biomass in the laboratory, *J. Geophys. Res.: Atmos.*, 2009, **114**, D19210.

7 S. P. Urbanski, M. C. Reeves, R. E. Corley, R. P. Silverstein and W. M. Hao, Contiguous United States wildland fire emission estimates during 2003–2015, *Earth Syst. Sci. Data*, 2018, **10**, 2241–2274.

8 S. L. Altshuler, Q. Zhang, M. T. Kleinman, F. Garcia-Menendez, C. T. Moore, M. L. Hough, E. D. Stevenson, J. C. Chow, D. A. Jaffe and J. G. Watson, Wildfire and prescribed burning impacts on air quality in the United States, *J. Air Waste Manage. Assoc.*, 2020, **70**, 961–970.

9 J. R. Laing and D. A. Jaffe, *Wildfires are causing extreme PM concentrations in the western U.S*, 2019, **https://pubs.awma.org/flip/EM-June-2019/jaffe.pdf**.

10 K. O'Dell, K. Bilsback, B. Ford, S. E. Martenies, S. Magzamen, E. V. Fischer and J. R. Pierce, Estimated Mortality and Morbidity Attributable to Smoke Plumes in the United States: Not Just a Western US Problem, *GeoHealth*, 2021, **5**, e2021GH000457.

11 S. O'Neill, S. Urbanski, S. Goodrick and S. Larkin, Smoke plumes: Emissions and effects, *Fire Manag. Today*, 2017, **75**, 10–15.

12 W. T. Sommers, R. A. Loehman and C. C. Hardy, Wildland fire emissions, carbon, and climate: Science overview and knowledge needs, *For. Ecol. Manage.*, 2014, **317**, 1–8.

13 C. C. Hardy, R. D. Ottmar, J. L. Peterson, J. E. Core and P. Seamon, *Smoke management guide for prescribed and wildland fire: 2001 edition*, PMS 420-2. NFES 1279, National Wildfire Coodination Group, Boise, ID, p. 226, 2001.

14 S. P. Urbanski, Combustion efficiency and emission factors for wildfire-season fires in mixed conifer forests of the northern Rocky Mountains, US, *Atmos. Chem. Phys.*, 2013, **13**, 7241–7262.

15 S. K. Akagi, I. R. Burling, A. Mendoza, T. J. Johnson, M. Cameron, D. W. T. Griffith, C. Paton-Walsh, D. R. Weise, J. Reardon and R. J. Yokelson, Field measurements of trace gases emitted by prescribed fires in southeastern US pine forests using an open-path FTIR system, *Atmos. Chem. Phys.*, 2014, **14**, 199–215.

16 NICC, National Interagency Coordination Center, *Wildland Fire Summary and Statistics Annual Report 2019*, 2019.

17 R. J. Yokelson, I. R. Burling, J. B. Gilman, C. Warneke, C. E. Stockwell, J. de Gouw, S. K. Akagi, S. P. Urbanski, P. Veres, J. M. Roberts, W. C. Kuster, J. Reardon, D. W. T. Griffith, T. J. Johnson, S. Hosseini, J. W. Miller, D. R. Cocker III, H. Jung and D. R. Weise, Coupling field and laboratory measurements to estimate the emission factors of identified and unidentified trace gases for prescribed fires, *Atmos. Chem. Phys.*, 2013, **13**, 89–116.

18 N. K. Scharko, A. M. Oeck, T. L. Myers, R. G. Tonkyn, C. A. Banach, S. P. Baker, E. N. Lincoln, J. Chong, B. M. Corcoran, G. M. Burke, R. D. Ottmar, J. C. Restaino, D. R. Weise and T. J. Johnson, Gas-phase pyrolysis products emitted by prescribed fires in pine forests with a shrub understory in the southeastern United States, *Atmos. Chem. Phys.*, 2019, **19**, 9681–9698.

19 I. R. Burling, R. J. Yokelson, D. W. T. Griffith, T. J. Johnson, P. Veres, J. M. Roberts, C. Warneke, S. P. Urbanski, J. Reardon, D. R. Weise, W. M. Hao and J. de Gouw, Laboratory measurements of trace gas emissions from biomass burning of fuel types from the southeastern and southwestern United States, *Atmos. Chem. Phys.*, 2010, **10**, 11115–11130.

20 A. A. May, G. R. McMeeking, T. Lee, J. W. Taylor, J. S. Craven, I. Burling, A. P. Sullivan, S. Akagi, J. L. Collett Jr, M. Flynn, H. Coe, S. P. Urbanski, J. H. Seinfeld, R. J. Yokelson and S. M. Kreidenweis, Aerosol emissions from prescribed fires in the United States: A synthesis of laboratory and aircraft measurements, *J. Geophys. Res.: Atmos.*, 2014, **119**, 11826–11849.

21 S. Urbanski, Wildland fire emissions, carbon, and climate: Emission factors, *For. Ecol. Manage.*, 2014, **317**, 51–60.

22 M. Fawaz, A. Avery, T. B. Onasch, L. R. Williams and T. C. Bond, Technical note: Pyrolysis principles explain time-resolved organic aerosol release from biomass burning, *Atmos. Chem. Phys.*, 2021, **21**, 15605–15618.

23 I. R. Burling, R. J. Yokelson, S. K. Akagi, S. P. Urbanski, C. E. Wold, D. W. T. Griffith, T. J. Johnson, J. Reardon and D. R. Weise, Airborne and ground-based measurements of the trace gases and particles emitted by prescribed fires in the United States, *Atmos. Chem. Phys.*, 2011, **11**, 12197–12216.

24 C. N. Jen, L. E. Hatch, V. Selimovic, R. J. Yokelson, R. Weber, A. E. Fernandez, N. M. Kreisberg, K. C. Barsanti and A. H. Goldstein, Speciated and total emission factors of particulate organics from burning western US wildland fuels and their dependence on combustion efficiency, *Atmos. Chem. Phys.*, 2019, **19**, 1013–1026.

25 S. K. Akagi, R. J. Yokelson, I. R. Burling, S. Meinardi, I. Simpson, D. R. Blake, G. R. McMeeking, A. Sullivan, T. Lee, S. Kreidenweis, S. Urbanski, J. Reardon, D. W. T. Griffith, T. J. Johnson and D. R. Weise, Measurements of reactive trace gases and variable O3 formation rates in some South Carolina biomass burning plumes, *Atmos. Chem. Phys.*, 2013, **13**, 1141–1165.

26 V. Selimovic, R. J. Yokelson, C. Warneke, J. M. Roberts, J. de Gouw, J. Reardon and D. W. T. Griffith, Aerosol optical properties and trace gas emissions by PAX and OP-FTIR for laboratory-simulated western US wildfires during FIREX, *Atmos. Chem. Phys.*, 2018, **18**, 2929–2948.

27 R. J. Yokelson, J. G. Goode, D. E. Ward, R. A. Susott, R. E. Babbitt, D. D. Wade, I. Bertschi, D. W. T. Griffith and W. M. Hao, Emissions of formaldehyde, acetic acid, methanol, and other trace gases from biomass fires in North Carolina measured by airborne Fourier transform infrared spectroscopy, *J. Geophys. Res.: Atmos.*, 1999, **104**, 30109–30125.

28 D. E. Ward and L. F. Radke, in *Fire in the Environment: The Ecological, Atmospheric, and Climatic Importance of Vegetation Fires. Dahlem Workshop Reports: Environmental Sciences Research Report 13*, ed. P. J. Crutzen and J. G. Goldammer, John Wiley & Sons., Chichester, England, 1993, pp. 53–76.

29 M. O. Andreae, Emission of trace gases and aerosols from biomass burning – an updated assessment, *Atmos. Chem. Phys.*, 2019, **19**, 8523–8546.

30 S. K. Akagi, R. J. Yokelson, C. Wiedinmyer, M. J. Alvarado, J. S. Reid, T. Karl, J. D. Crounse and P. O. Wennberg, Emission factors for open and domestic biomass burning for use in atmospheric models, *Atmos. Chem. Phys.*, 2011, **11**, 4039–4072.

31 S. J. Prichard, S. M. O'Neill, P. Eagle, A. G. Andreu, B. Drye, J. Dubowy, S. Urbanski and T. M. Strand, Wildland fire emission factors in North America: synthesis of existing data, measurement needs and management applications, *Int. J. Wildland Fire*, 2020, **29**, 132–147.

32 Q. Chen, C. L. Heald, J. L. Jimenez, M. R. Canagaratna, Q. Zhang, L.-Y. He, X.-F. Huang, P. Campuzano-Jost, B. B. Palm, L. Poulain, M. Kuwata, S. T. Martin, J. P. D. Abbatt, A. K. Y. Lee and J. Liggio, Elemental composition of organic aerosol: The gap between ambient and laboratory measurements, *Geophys. Res. Lett.*, 2015, **42**, 4182–4189.

33 A. L. Holder, G. S. W. Hagler, J. Aurell, M. D. Hays and B. K. Gullett, Particulate matter and black carbon optical properties and emission factors from prescribed fires in the southeastern United States, *J. Geophys. Res.: Atmos.*, 2016, **121**, 3465–3483.

34 R. W. Long, A. Whitehill, A. Habel, S. Urbanski, H. Halliday, M. Colón, S. Kaushik and M. S. Landis, Comparison of ozone measurement methods in biomass burning smoke: an evaluation under field and laboratory conditions, *Atmos. Meas. Tech.*, 2021, **14**, 1783–1800.

35 J. Aurell, B. K. Gullett and D. Tabor, Emissions from southeastern U.S. Grasslands and pine savannas: Comparison of aerial and ground field measurements with laboratory burns, *Atmos. Environ.*, 2015, **111**, 170–178.

36 X. Liu, L. G. Huey, R. J. Yokelson, V. Selimovic, I. J. Simpson, M. Müller, J. L. Jimenez, P. Campuzano-Jost, A. J. Beyersdorf, D. R. Blake, Z. Butterfield, Y. Choi, J. D. Crounse, D. A. Day, G. S. Diskin, M. K. Dubey, E. Fortner, T. F. Hanisco, W. Hu, L. E. King, L. Kleinman, S. Meinardi, T. Mikoviny, T. B. Onasch, B. B. Palm, J. Peischl, I. B. Pollack, T. B. Ryerson, G. W. Sachse, A. J. Sedlacek, J. E. Shilling, S. Springston, J. M. St. Clair, D. J. Tanner, A. P. Teng, P. O. Wennberg, A. Wisthaler and G. M. Wolfe, Airborne measurements of western U.S. wildfire emissions: Comparison with prescribed burning and air quality implications, *J. Geophys. Res.: Atmos.*, 2017, **122**, 6108–6129.

37 F. Fachinger, F. Drewnick and S. Borrmann, How villages contribute to their local air quality – The influence of traffic- and biomass combustion-related emissions assessed by mobile mappings of PM and its components, *Atmos. Environ.*, 2021, **263**, 118648.

38 S. Prichard, N. S. Larkin, R. Ottmar, N. H. F. French, K. Baker, T. Brown, C. Clements, M. Dickinson, A. Hudak, A. Kochanski, R. Linn, Y. Liu, B. Potter, W. Mell, D. Tanzer, S. Urbanski and A. Watts, The Fire and Smoke Model Evaluation Experiment—A Plan for Integrated, Large Fire–Atmosphere Field Campaigns, *Atmosphere*, 2019, **10**(2), 66.

39 M. A. Carroll, S. B. Bertman and P. B. Shepson, Overview of the Program for Research on Oxidants: PHotochemistry, Emissions, and Transport (PROPHET) summer 1998 measurements intensive, *J. Geophys. Res.: Atmos.*, 2001, **106**, 24275–24288.

40 K. M. Bergen and I. Dronova, Observing succession on aspen-dominated landscapes using a remote sensing-ecosystem approach, *Landsc. Ecol.*, 2007, **22**, 1395–1410.

41 C. M. Gough, B. S. Hardiman, L. E. Nave, G. Bohrer, K. D. Maurer, C. S. Vogel, K. J. Nadelhoffer and P. S. Curtis, Sustained carbon uptake and storage following moderate disturbance in a Great Lakes forest, *Ecol Appl*, 2013, **23**, 1202–1215.

42 C. E. Kolb, S. C. Herndon, J. B. McManus, J. H. Shorter, M. S. Zahniser, D. D. Nelson, J. T. Jayne, M. R. Canagaratna and D. R. Worsnop, Mobile Laboratory with Rapid Response Instruments for Real-Time Measurements of Urban and Regional Trace Gas and

Particulate Distributions and Emission Source Characteristics, *Environ. Sci. Technol.*, 2004, **38**, 5694–5703.

43 S. C. Herndon, J. T. Jayne, M. S. Zahniser, D. R. Worsnop, B. Knighton, E. Alwine, B. K. Lamb, M. Zavala, D. D. Nelson, J. B. McManus, J. H. Shorter, M. R. Canagaratna, T. B. Onasch and C. E. Kolb, Characterization of urban pollutant emission fluxes and ambient concentration distributions using a mobile laboratory with rapid response instrumentation, *Faraday Discuss.*, 2005, **130**, 327–339.

44 S. B. Wales, M. R. Kreider, J. Atkins, C. M. Hulshof, R. T. Fahey, L. E. Nave, K. J. Nadelhoffer and C. M. Gough, Stand age, disturbance history and the temporal stability of forest production, *For. Ecol. Manage.*, 2020, **460**, 117865.

45 E. J. Dunlea, S. C. Herndon, D. D. Nelson, R. M. Volkamer, F. San Martini, P. M. Sheehy, M. S. Zahniser, J. H. Shorter, J. C. Wormhoudt, B. K. Lamb, E. J. Allwine, J. S. Gaffney, N. A. Marley, M. Grutter, C. Marquez, S. Blanco, B. Cardenas, A. Retama, C. R. Ramos Villegas, C. E. Kolb, L. T. Molina and M. J. Molina, Evaluation of nitrogen dioxide chemiluminescence monitors in a polluted urban environment, *Atmos. Chem. Phys.*, 2007, **7**, 2691–2704.

46 T. I. Yacovitch, S. C. Herndon, J. R. Roscioli, C. Floerchinger, R. M. McGovern, M. Agnese, G. Pétron, J. Kofler, C. Sweeney, A. Karion, S. A. Conley, E. A. Kort, L. Nähle, M. Fischer, L. Hildebrandt, J. Koeth, J. B. McManus, D. D. Nelson, M. S. Zahniser and C. E. Kolb, Demonstration of an Ethane Spectrometer for Methane Source Identification, *Environ. Sci. Technol.*, 2014, **48**, 8028–8034.

47 J. B. McManus, M. S. Zahniser, D. D. Nelson, J. H. Shorter, S. C. Herndon, D. Jervis, M. Agnese, R. McGovern, T. I. Yacovitch and J. R. Roscioli, Recent progress in laser-based trace gas instruments: performance and noise analysis, *Appl. Phys. B: Lasers Opt.*, 2015, **119**, 203–218.

48 A. K. Y. Lee, M. D. Willis, R. M. Healy, T. B. Onasch and J. P. D. Abbatt, Mixing state of carbonaceous aerosol in an urban environment: single particle characterization using the soot particle aerosol mass spectrometer (SP-AMS), *Atmos. Chem. Phys.*, 2015, **15**, 1823–1841.

49 T. B. Onasch, A. Trimborn, E. C. Fortner, J. T. Jayne, G. L. Kok, L. R. Williams, P. Davidovits and D. R. Worsnop, Soot Particle Aerosol Mass Spectrometer: Development, Validation, and Initial Application, *Aerosol Sci. Technol.*, 2012, **46**, 804–817.

50 M. D. Willis, R. M. Healy, N. Riemer, M. West, J. M. Wang, C. H. Jeong, J. C. Wenger, G. J. Evans, J. P. D. Abbatt and A. K. Y. Lee, Quantification of black carbon mixing state from traffic: implications for aerosol optical properties, *Atmos. Chem. Phys.*, 2016, **16**, 4693–4706.

51 M. O. Andreae and P. Merlet, Emission of trace gases and aerosols from biomass burning, *Global Biogeochem. Cycles*, 2001, **15**, 955–966.

52 K. A. Pratt, J. E. Mayer, J. C. Holecek, R. C. Moffet, R. O. Sanchez, T. P. Rebotier, H. Furutani, M. Gonin, K. Fuhrer, Y. Su, S. Guazzotti and K. A. Prather, Development and Characterization of an Aircraft Aerosol Time-of-Flight Mass Spectrometer, *Anal. Chem.*, 2009, **81**, 1792–1800.

53 M. J. Gunsch, R. M. Kirpes, K. R. Kolesar, T. E. Barrett, S. China, R. J. Sheesley, A. Laskin, A. Wiedensohler, T. Tuch and K. A. Pratt, Contributions of transported Prudhoe Bay oil field emissions to the aerosol population in Utqiaġvik, Alaska, *Atmos. Chem. Phys.*, 2017, **17**, 10879–10892.

54 C. M. Sultana, G. C. Cornwell, P. Rodriguez and K. A. Prather, FATES: a flexible analysis toolkit for the exploration of single-particle mass spectrometer data, *Atmos. Meas. Tech.*, 2017, **10**, 1323–1334.

55 X.-H. Song, P. K. Hopke, D. P. Fergenson and K. A. Prather, Classification of Single Particles Analyzed by ATOFMS Using an Artificial Neural Network, ART-2A, *Anal. Chem.*, 1999, **71**, 860–865.

56 K. A. Pratt and K. A. Prather, Real-Time, Single-Particle Volatility, Size, and Chemical Composition Measurements of Aged Urban Aerosols, *Environ. Sci. Technol.*, 2009, **43**, 8276–8282.

57 K. A. Pratt, S. M. Murphy, R. Subramanian, P. J. DeMott, G. L. Kok, T. Campos, D. C. Rogers, A. J. Prenni, A. J. Heymsfield, J. H. Seinfeld and K. A. Prather, Flight-based chemical characterization of biomass burning aerosols within two prescribed burn smoke plumes, *Atmos. Chem. Phys.*, 2011, **11**, 12549–12565.

58 M. D. Zauscher, Y. Wang, M. J. K. Moore, C. J. Gaston and K. A. Prather, Air Quality Impact and Physicochemical Aging of Biomass Burning Aerosols during the 2007 San Diego Wildfires, *Environ. Sci. Technol.*, 2013, **47**, 7633–7643.

59 P. J. Silva, D.-Y. Liu, C. A. Noble and K. A. Prather, Size and Chemical Characterization of Individual Particles Resulting from Biomass Burning of Local Southern California Species, *Environ. Sci. Technol.*, 1999, **33**, 3068–3076.

60 M. J. Gunsch, N. W. May, M. Wen, C. L. H. Bottenus, D. J. Gardner, T. M. VanReken, S. B. Bertman, P. K. Hopke, A. P. Ault and K. A. Pratt, Ubiquitous influence of wildfire emissions and secondary organic aerosol on summertime atmospheric aerosol in the forested Great Lakes region, *Atmos. Chem. Phys.*, 2018, **18**, 3701–3715.

61 J. S. Reid, R. Koppmann, T. F. Eck and D. P. Eleuterio, A review of biomass burning emissions part II: intensive physical properties of biomass burning particles, *Atmos. Chem. Phys.*, 2005, **5**, 799–825.

62 W. M. Hao and D. E. Ward, Methane production from global biomass burning, *J. Geophys. Res.: Atmos.*, 1993, **98**, 20657–20661.

63 C. E. Stockwell, R. J. Yokelson, S. M. Kreidenweis, A. L. Robinson, P. J. DeMott, R. C. Sullivan, J. Reardon, K. C. Ryan, D. W. T. Griffith and L. Stevens, Trace gas emissions from combustion of peat, crop residue, domestic biofuels, grasses, and other fuels: configuration and Fourier transform infrared (FTIR) component of the fourth Fire Lab at Missoula Experiment (FLAME-4), *Atmos. Chem. Phys.*, 2014, **14**, 9727–9754.

64 M. Becidan, Ø. Skreiberg and J. E. Hustad, NO_x and N_2O Precursors (NH_3 and HCN) in Pyrolysis of Biomass Residues, *Energy Fuels*, 2007, **21**, 1173–1180.

65 P. J. Crutzen, L. E. Heidt, J. P. Krasnec, W. H. Pollock and W. Seiler, Biomass burning as a source of atmospheric gases CO, H_2, N_2O, NO, CH_3Cl and COS, *Nature*, 1979, **282**, 253–256.

66 J. S. King, C. P. Giardina, K. S. Pregitzer and A. L. Friend, Biomass partitioning in red pine (Pinus resinosa) along a chronosequence in the Upper Peninsula of Michigan, *Can. J. For. Res.*, 2007, **37**, 93–102.

67 E. Fortner, T. Onasch, M. Canagaratna, L. R. Williams, T. Lee, J. Jayne and D. Worsnop, Examining the chemical composition of black carbon particles from biomass burning with SP-AMS, *J. Aerosol Sci.*, 2018, **120**, 12–21.

68 L. A. Garofalo, M. A. Pothier, E. J. T. Levin, T. Campos, S. M. Kreidenweis and D. K. Farmer, Emission and Evolution of Submicron Organic Aerosol in Smoke from Wildfires in the Western United States, *ACS Earth Space Chem.*, 2019, **3**, 1237–1247.

69 S. Zhou, S. Collier, D. A. Jaffe, N. L. Briggs, J. Hee, A. J. Sedlacek Iii, L. Kleinman, T. B. Onasch and Q. Zhang, Regional influence of wildfires on aerosol chemistry in the western US and insights into atmospheric aging of biomass burning organic aerosol, *Atmos. Chem. Phys.*, 2017, **17**, 2477–2493.

70 J. Aurell and B. K. Gullett, Emission Factors from Aerial and Ground Measurements of Field and Laboratory Forest Burns in the Southeastern U.S.: PM2.5, Black and Brown Carbon, VOC, and PCDD/PCDF, *Environ. Sci. Technol.*, 2013, **47**, 8443–8452.

71 M. F. Heringa, P. F. DeCarlo, R. Chirico, A. Lauber, A. Doberer, J. Good, T. Nussbaumer, A. Keller, H. Burtscher, A. Richard, B. Miljevic, A. S. H. Prevot and U. Baltensperger, Time-Resolved Characterization of Primary Emissions from Residential Wood Combustion Appliances, *Environ. Sci. Technol.*, 2012, **46**, 11418–11425.

72 B. B. Palm, Q. Peng, C. D. Fredrickson, B. H. Lee, L. A. Garofalo, M. A. Pothier, S. M. Kreidenweis, D. K. Farmer, R. P. Pokhrel, Y. Shen, S. M. Murphy, W. Permar, L. Hu, T. L. Campos, S. R. Hall, K. Ullmann, X. Zhang, F. Flocke, E. V. Fischer and J. A. Thornton, Quantification of organic aerosol and brown carbon evolution in fresh wildfire plumes, *Proc. Natl. Acad. Sci. U. S. A.*, 2020, **117**, 29469.

73 A. R. Martin, S. Gezahegn and S. C. Thomas, Variation in carbon and nitrogen concentration among major woody tissue types in temperate trees, *Can. J. For. Res.*, 2015, **45**, 744–757.

74 J. D. McDonald, B. Zielinska, E. M. Fujita, J. C. Sagebiel, J. C. Chow and J. G. Watson, Fine Particle and Gaseous Emission Rates from Residential Wood Combustion, *Environ. Sci. Technol.*, 2000, **34**, 2080–2091.

75 A. Akherati, Y. He, M. M. Coggon, A. R. Koss, A. L. Hodshire, K. Sekimoto, C. Warneke, J. de Gouw, L. Yee, J. H. Seinfeld, T. B. Onasch, S. C. Herndon, W. B. Knighton, C. D. Cappa, M. J. Kleeman, C. Y. Lim, J. H. Kroll, J. R. Pierce and S. H. Jathar, Oxygenated Aromatic Compounds are Important Precursors of Secondary Organic Aerosol in Biomass-Burning Emissions, *Environ. Sci. Technol.*, 2020, **54**, 8568–8579.

76 E. A. Bruns, I. El Haddad, J. G. Slowik, D. Kilic, F. Klein, U. Baltensperger and A. S. H. Prévôt, Identification of significant precursor gases of secondary organic aerosols from residential wood combustion, *Sci. Rep.*, 2016, **6**, 27881.

77 A. K. Y. Lee, M. D. Willis, R. M. Healy, J. M. Wang, C. H. Jeong, J. C. Wenger, G. J. Evans and J. P. D. Abbatt, Single-particle characterization of biomass burning organic aerosol (BBOA): evidence for non-uniform mixing of high molecular weight organics and potassium, *Atmos. Chem. Phys.*, 2016, **16**, 5561–5572.

78 J. Li, M. Pósfai, P. V. Hobbs and P. R. Buseck, Individual aerosol particles from biomass burning in southern Africa: 2, Compositions and aging of inorganic particles, *J. Geophys. Res.: Atmos.*, 2003, **108**, 8484.

79 P. K. Hudson, D. M. Murphy, D. J. Cziczo, D. S. Thomson, J. A. de Gouw, C. Warneke, J. Holloway, H.-J. Jost and G. Hübler, Biomass-burning particle measurements: Characteristic composition and chemical processing, *J. Geophys. Res.: Atmos.*, 2004, **109**, D23S27.

80 J. Pagels, D. D. Dutcher, M. R. Stolzenburg, P. H. McMurry, M. E. Gälli and D. S. Gross, Fine-particle emissions from solid biofuel combustion studied with single-particle mass spectrometry: Identification of markers for organics, soot, and ash components, *J. Geophys. Res.: Atmos.*, 2013, **118**, 859–870.

81 E. Gard, J. E. Mayer, B. D. Morrical, T. Dienes, D. P. Fergenson and K. A. Prather, Real-Time Analysis of Individual Atmospheric Aerosol Particles: Design and Performance of a Portable ATOFMS, *Anal. Chem.*, 1997, **69**, 4083–4091.

82 M. T. Spencer and K. A. Prather, Using ATOFMS to Determine OC/EC Mass Fractions in Particles, *Aerosol Sci. Technol.*, 2006, **40**, 585–594.

83 M. T. Baeza-Romero, J. M. Wilson, E. M. Fitzpatrick, J. M. Jones and A. Williams, In Situ Study of Soot from the Combustion of a Biomass Pyrolysis Intermediate—Eugenol—and *n*-Decane Using Aerosol Time of Flight Mass Spectrometry, *Energy Fuels*, 2010, **24**, 439–445.

84 E. M. Fitzpatrick, J. M. Jones, M. Pourkashanian, A. B. Ross, A. Williams and K. D. Bartle, Mechanistic Aspects of Soot Formation from the Combustion of Pine Wood, *Energy Fuels*, 2008, **22**, 3771–3778.

85 M. Dall'Osto and R. M. Harrison, Urban organic aerosols measured by single particle mass spectrometry in the megacity of London, *Atmos. Chem. Phys.*, 2012, **12**, 4127–4142.

86 D. A. Sodeman, S. M. Toner and K. A. Prather, Determination of Single Particle Mass Spectral Signatures from Light-Duty Vehicle Emissions, *Environ. Sci. Technol.*, 2005, **39**, 4569–4580.

87 D. S. Gross, M. E. Galli, P. J. Silva, S. H. Wood, D.-Y. Liu and K. A. Prather, Single Particle Characterization of Automobile

and Diesel Truck Emissions in the Caldecott Tunnel, *Aerosol Sci. Technol.*, 2000, **32**, 152–163.

88 J. M. Wilson, M. T. Baeza-Romero, J. M. Jones, M. Pourkashanian, A. Williams, A. R. Lea-Langton, A. B. Ross and K. D. Bartle, Soot Formation from the Combustion of Biomass Pyrolysis Products and a Hydrocarbon Fuel, n-Decane: An Aerosol Time Of Flight Mass Spectrometer (ATOFMS) Study, *Energy Fuels*, 2013, **27**, 1668–1678.

89 P. J. Silva and K. A. Prather, Interpretation of Mass Spectra from Organic Compounds in Aerosol Time-of-Flight Mass Spectrometry, *Anal. Chem.*, 2000, **72**, 3553–3562.

90 M. A. Bari, G. Baumbach, J. Brodbeck, M. Struschka, B. Kuch, W. Dreher and G. Scheffknecht, Characterisation of particulates and carcinogenic polycyclic aromatic hydrocarbons in wintertime wood-fired heating in residential areas, *Atmos. Environ.*, 2011, **45**, 7627–7634.

91 M. Elsasser, C. Busch, J. Orasche, C. Schön, H. Hartmann, J. Schnelle-Kreis and R. Zimmermann, Dynamic Changes of the Aerosol Composition and Concentration during Different Burning Phases of Wood Combustion, *Energy Fuels*, 2013, **27**, 4959–4968.